Nano Res (2009) 2: 955–965
DOI 10.1007/s12274-009-9098-4
Research Article

Enhanced Antibacterial Activity of Bifunctional Fe_3O_4–Ag Core–Shell Nanostructures

Bhupendra Chudasama [1] (✉), Anjana K. Vala[2], Nidhi Andhariya[2], R. V. Upadhyay[3], and R. V. Mehta[2] (✉)

[1] Department of Applied Physics, S.V. National Institute of Technology, Surat 395007, India
[2] Department of Physics, Bhavnagar University, Bhavnagar 364022, India
[3] P.D. Patel Institute of Applied Sciences, Charotar University of Science and Technology, Education campus, Changa 388421, India

Received: 3 September 2009 / Revised: 18 October 2009 / Accepted: 21 October 2009

ABSTRACT

We describe a simple one-pot thermal decomposition method for the production of a stable colloidal suspension of narrowly dispersed superparamagnetic Fe_3O_4–Ag core–shell nanostructures. These biocompatible nanostructures are highly toxic to microorganisms. Antimicrobial activity studies were carried out on both Gram negative (*Escherichia coli* and *Proteus vulgaris*) and Gram positive (*Bacillus megaterium* and *Staphylococcus aureus*) bacterial strains. Efforts have been made to understand the underlying molecular mechanism of such antibacterial actions. The effect of the core–shell nanostructures on Gram negative strains was found to be better than that observed for silver nanoparticles. The minimum inhibitory concentration (MIC) values of these nanostructures were found to be considerably lower than those of commercially available antibiotics. We attribute this enhanced antibacterial effect of the nanostructures to their stability as a colloid in the medium, which modulates the phosphotyrosine profile of the bacterial proteins and arrests bacterial growth. We also demonstrate that these core–shell nanostructures can be removed from the medium by means of an external magnetic field which provides a mechanism to prevent uncontrolled waste disposal of these potentially hazardous nanostructures.

KEYWORDS

Core-shell nanostructure, antimicrobial activity, minimum inhibitory concentration, phase transfer

Introduction

The appearance of new strains of bacteria resistant to current antibiotics [1] has become a serious problem in public healthcare. For example, MRSA bacteria kill 5000 hospital patients a year in the UK alone and any method of attacking them, not involving antibiotics, is becoming increasingly important. Therefore, there is a strong incentive to develop new bactericides [2]. Silver may have an important advantage over conventional antibiotics as it kills all pathogenic microorganisms, and no organism has ever been reported to readily develop resistance to it. Furthermore, microbes are unlikely to develop resistance against silver, as they do against conventional and narrow-target antibiotics, because the metal attacks a broad range of targets in the organisms, which means that they would have to

Address correspondence to Bhupendra Chudasama, bnc_ta@ashd. svnit.ac.in; R. V. Mehta, rvm@bhavuni.edu

develop a host of mutations simultaneously, in order to protect themselves. For these reasons silver-based compounds have been used extensively in many bactericidal applications [3, 4]. Silver compounds have also been used in the medical field to treat burns and a variety of infections [5]. Several salts of silver and their derivatives are commercially employed as antimicrobial agents [6].

Ultimately, these products end up in the environment during waste disposal. However, there are potential risks involved in using these ultra-fine silver particles for medicinal purposes, as it is very difficult to remove colloidal silver by virtue of its chemical and physical properties. Silver is a recognized cause of argyrosis and argyria [7, 8], and clinical toxicity of silver to mammiferous cells has also been reported [9–11]. Therefore, maximum contamination levels for silver in drinking water (100 ppb) [12] and the occupational exposure limit to the various forms of silver (0.01 mg/m^3) [13] have been established in order to avoid the accumulation of silver in the human body. In order to improve scientific data and to enhance our insight into the health and environmental impact of silver nanoparticles, scientists in Singapore initiated an *in vivo* toxicology study to examine nanosilver in a zebrafish model [11]. They concluded that silver nanoparticles have the potential to give rise to health and ecotoxicity issues in a concentration-dependent manner.

One approach to overcome these problems is to use nanomagnetic system as a core and silver nanoparticles as the shell, and utilize the resulting core–shell nanostructures for antimicrobial activity in their colloidal state and subsequently remove them from the medium by means of an external magnetic field. However, the bactericidal property of these nanoparticles depends on their stability in the medium, since this determines the retention time for bacterium–nanoparticle interactions. Therefore, the preparation of core–shell nanostructures of silver, stable enough to significantly restrict bacterial growth, remains a significant challenge.

In the present investigation, we describe a single pot synthesis protocol for the synthesis of a colloidal suspension of ultrafine, narrowly dispersed core–shell nanostructures of Fe_3O_4–Ag. The antibacterial activity of the bifunctional colloid was tested against Gram positive and Gram negative bacterial strains. The effect of the nanostructures was found to be significantly more pronounced on *E. coli* (Gram negative) compared with the other tested microorganisms. These core–shell nanostructures can be successfully removed from the medium by a static magnetic field which provides a mechanism to prevent uncontrolled waste disposal of these potentially hazardous nanostructures.

1. Experimental

1.1 Materials

Silver nitrate (99.8%), AR grade hexane, oleic acid, and biphenyl ether were produred from S. D. Fine-Chem Ltd. 1,2-hexadecanediol (90%), iron(Ⅲ) acetylacetonate ($Fe(acac)_3$) (99.9%), Pluronic F-127 and oleylamine were obtained from Aldrich. Absolute ethanol (99.9%) was supplied by Hayman Ltd. and acetone (99%) was purchased from Merck. Nutrient broth medium was obtained from Himedia. Aqueous solutions were prepared in High performance liquid chromatography (HPLC) grade water, which was procured from Merck. All the chemicals were used as received without any further purification. The cultures (*Bacillus megaterium*, *Staphylococcus aureus*, *Escherichia coli*, and *Proteus vulgaris*) were gifted by the Microbiology Department of Sir P. P. Institute of Science, Bhavnagar University, India.

1.2 Synthesis of Fe_3O_4 and Fe_3O_4–Ag core–shell nanostructures

Monodisperse magnetic nanoparticles of Fe_3O_4 were prepared by following the thermal decomposition method developed by Sun et al. [14, 15]. Briefly, $Fe(acac)_3$ (2 mmol), 1,2-hexadecanediol (10 mmol), oleic acid (6 mmol), oleylamine (6 mmol), and biphenyl ether (20 mL) were mixed and stirred magnetically in a 150 mL three neck flask equipped with a condenser. The mixture was gradually heated to 200 °C ± 2 °C at a rate of 3 °C/min and maintained at that temperature for 2 h. A black-brown mixture was formed, indicating the nucleation of Fe_3O_4 nanocrystals. The reaction temperature was raised to 260 °C ± 3 °C at a steady rate of 2 °C/min and

refluxed for another hour to allow the nuclei to grow. The suspension of nanoparticles was divided equally into two fractions after reducing the temperature to 180 °C. One fraction was cooled to room temperature, while a silver shell was formed on the other fraction of Fe_3O_4 nanoparticles.

The silver coating was formed on the Fe_3O_4 nanoparticles by directly reducing $AgNO_3$ with oleylamine onto the surface of the Fe_3O_4 nanoparticles. The oleylamine and $AgNO_3$ were injected into the reaction mixture at 180 °C. The w/w ratio of oleylamine to silver nitrate was 0.81:100 and Ag to Fe_3O_4 was 1:0.3. The mixture was allowed to reflux at 180 °C ± 2 °C for 2 h in order to produce homogeneous nucleation of Ag. The reaction temperature was lowered to 150 °C ± 2 °C and the mixture was maintained at that temperature for another 6 h to allow formation of a silver shell on the Fe_3O_4 core. Finally, the resulting black mixture was cooled to room temperature.

Fe_3O_4 nanoparticles and Fe_3O_4–Ag core–shell nanostructures were precipitated with absolute ethanol. The precipitates were recovered from the solution by magnetic decantation after several washes with ethanol. To remove the excess surfactants and impurities, a precipitation–redispersion procedure was adopted. Both the precipitates were redispersed in 40 mL hexane and the dispersions were centrifuged at 6000 rpm for 10 min. Undispersed residues (if any) were removed and each dispersed phase was further divided into two equal fractions. One fraction each of Fe_3O_4 nanoparticles and Fe_3O_4–Ag nanostructures was again precipitated with 20 mL absolute ethanol. The precipitates were then isolated by magnetic decantation and dried at room temperature. The dispersed phases of Fe_3O_4 and Fe_3O_4–Ag were preserved for further processing/analysis.

1.3 Phase transfer of hydrophobic Fe_3O_4–Ag nanostructures via ligand exchange

The oleylamine coating on the surface of the nanoparticles makes them hydrophobic. However, hydrophilic nature is an essential criterion for biological applicability of nanoparticles. Hence, we have developed a facile phase transfer mechanism to produce water-dispersible Fe_3O_4–Ag core–shell nanostructures by using the block copolymer Pluronic F-127. 20 mL of a 0.1 mol/L aqueous solution of Pluronic F-127 was mixed with an equal volume of stock solution of Fe_3O_4–Ag nanostructures in hexane in a 100 mL beaker, which was covered with a perforated aluminum foil to control the evaporation of hexane. The mixture was mechanically stirred until the organic phase was evaporated completely.

To confirm the phase transfer of the Fe_3O_4–Ag nanostructures, an equal volume of fresh hexane solution was poured into the resulting aqueous solution of Fe_3O_4–Ag. Successful phase transfer was indicated by aqueous and organic phases remaining immiscible with the latter remaining colorless.

1.4 Investigation of Fe_3O_4 and Fe_3O_4–Ag nanostructures

Structural investigation of Fe_3O_4 and Fe_3O_4–Ag nanostructures was carried out by recording their powder X-ray diffraction patterns. The patterns were recorded on a Bruker D8 Advance X-ray diffractometer at room temperature (300 K) using monochromatic Cu Kα radiation (λ =0.15406 nm). Transmission electron microscopy images and energy dispersive X-ray spectra (EDS) were obtained on JEOL (Model GEM 200) transmission electron microscope operated at 200 kV. For this purpose, a fine drop of Fe_3O_4 nanoparticles and Fe_3O_4–Ag nanostructures dispersed in hexane were placed on carbon-coated copper grids and the hexane was allowed to evaporate slowly at room temperature. The elemental concentration of Ag and Fe in the core–shell nanostructures was determined by inductively coupled plasma atomic emission spectroscopy (ICP–AES). The measurements were carried out on a Perkin Elmer Optima 2000 ICP–AES instrument. UV–vis spectra of Fe_3O_4 and Fe_3O_4–Ag dispersed in hexane and water were recorded on an Elico biospectrophotometer (model BL198). Magnetic properties were determined at room temperature on a home made vibrating sample magnetometer (VSM). The sensitivity of the magnetometer is 10^{-6} emu/g and it was calibrated against a nickel standard.

1.5 Antibacterial activity

Antimicrobial activity of the synthesized

nanostructures was tested against four bacteria, two Gram positive—*Bacillus megaterium*, *Staphylococcus aureus*—and two Gram negative *E. coli* and *Proteus vulgaris*. The minimum inhibitory concentration (MIC) values of the core–shell nanostructures for the test microorganisms were determined. The MIC is the concentration required to completely inhibit the bacterial growth.

Four sets of 10 mL nutrient broth medium containing Fe_3O_4–Ag nanostructures with effective silver concentrations of 0, 5, 10,…,400 μg/mL were prepared. The mass ratio of Fe:Ag obtained from the ICP-AES analysis was used to determine the effective silver concentration in the core–shell nanostructures. Each set was inoculated aseptically with 10 μL of the respective bacterial suspension (approximately 1×10^8 colony forming units (CFU)/mL). The inoculated sets were incubated at 37 °C for 24 h. The experiments were carried out in triplicate. Evaluation of the MIC was done by visual inspection of growth/no growth in mixtures containing different concentrations of nanostructures. The lowest concentration of silver that inhibited bacterial growth was taken as the MIC for that particular bacterium. Control experiments were also executed to investigate the antibacterial activity of Fe_3O_4 nanoparticles.

1.6 Isolation of nanostructures from the medium

Fe_3O_4–Ag nanostructures were isolated from the bacterial medium by filtering it with a steel wool filter under a static magnetic field of 2000 Oe. The constant static magnetic field was produced with an electromagnet. The filter was kept at the center of the pole pieces of an electromagnet, and the medium containing Fe_3O_4–Ag nanostructures was allowed to pass through it, when the magnetic field was ON. The filtered medium was collected and examined for the presence of nanostructures by UV–vis spectroscopy.

2. Results and discussion

2.1 Synthesis of Fe_3O_4 and Fe_3O_4–Ag core–shell nanostructures

Synthesis of Fe_3O_4 magnetic nanoparticles was carried out by following the protocols developed by Sun et al. [14, 15]. To achieve the required monodispersity in size, it is necessary to isolate nucleation and growth stages [15]. The optimum time for homogeneous nucleation and sustained growth was determined experimentally.

Silver nanoparticles can be produced by chemical reduction of silver ions with [16] and without [17] stabilizing agents, thermal decomposition in organic solvents [18], and chemical and photoreduction in reverse micelles [19]. Recently, Hiramatsu [20] and Chen et al. [21] have developed a versatile technique to produce highly monodisperse silver nanoparticles by using toluene/hexane or liquid paraffin as a solvent. In our method, to avoid solvent exchange, we have used biphenyl ether as a single solvent for the syntheses of both the Fe_3O_4 core and the Ag shell. It was reported earlier that Oswald ripening is necessary to produce narrowly dispersed nanoparticles of noble metals [21]. Therefore, in the last stage of preparation, the reaction temperature was lowered to 150 °C, as it is known that ripening at lower temperature will afford better control over the growth rate of individual crystallites. Therefore, when the system temperature is lowered and the system allowed to ripen, larger size nuclei will grow further in size at the cost of smaller ones, i.e., smaller size nuclei will dissolve in the medium, which will provide favorable conditions for homogeneous growth of the silver shell. The choice of oleylamine as capping and reducing agent for the formation of silver shell was made as oleylamine was already present in the reaction mixture from the first stage and so did not require the addition of a further component.

2.2 Phase transfer of hydrophobic Fe_3O_4–Ag nanostructures via ligand exchange

The block copolymer, Pluronic F-127 was used to transfer hydrophobic Fe_3O_4–Ag nanostructures into aqueous medium. In the first step, Pluronic F-127 replaces the original oleylamine ligands on the surface of nanostructures and becomes the new ligand due to the complexation interaction between Pluronic and oleylamine, while in the second step, Pluronic F-127-capped nanostructures are transferred into the aqueous medium due to the hydrophilic

nature of the capping agent. In this experiment, hexane was successfully used as a medium to achieve exchange between the original hydrophobic ligands (oleylamine) and Pluronic F-127.

Figure 1 shows images of the original (a) and phase-transferred (b) nanostructures dispersed in the two media. The upper medium is hexane and the lower one is water in each case. The original hydrophobic nanostructures were easily dispersed in hexane (a). By exchanging the original ligands (oleylamine) with block copolymer Pluronic F-127, the transferred nanostructures exhibited good stability in water (b), even after being washed with hexane.

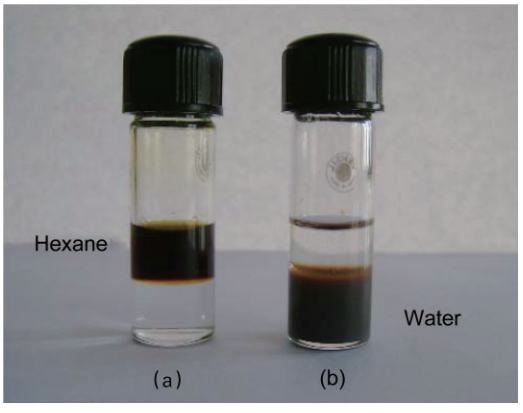

Figure 1 Photograph showing the successful phase transfer of oleylamine (hydrophobic) capped Fe_3O_4–Ag nanostructures from hexane into water using the block copolymer Pluronic F-127 (hydrophilic): (a) before phase transfer (dispersed in hexane) and (b) after phase transfer (dispersed in water)

2.3 Investigation of Fe_3O_4 and Fe_3O_4–Ag nanostructures

Figure 2 shows the X-ray diffraction patterns of Fe_3O_4 and Fe_3O_4–Ag nanostructures. All six peaks in the pattern of Fe_3O_4 can be indexed to the fcc inverse spinel structure (Fig. 2(a)). The value of the lattice parameter obtained from the most intense peak (311) was found to be 0.837 nm. This result is in good agreement with that reported in the powder diffraction database (JCPDS Card No. 19-0629).

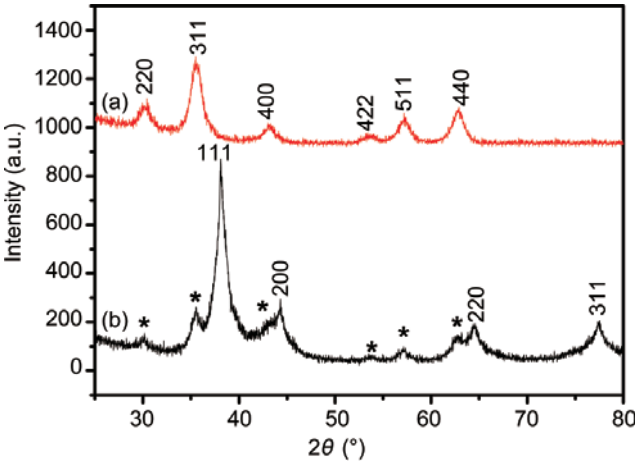

Figure 2 X-ray diffraction patterns of (a) Fe_3O_4 and (b) Fe_3O_4–Ag nanostructures. The reflections marked with an asterisk (*) sign in the diffraction pattern of Fe_3O_4–Ag (b) correspond to the inverse spinel structure of the Fe_3O_4 core and the indexed reflections are due to the fcc structure of the silver shell

Ten peaks are observed in the XRD spectrum of Fe_3O_4–Ag core–shell nanostructures. Six of them can again be indexed well to the fcc inverse spinel structure of Fe_3O_4 core. They are marked with an asterisk sign (*) in the spectrum (Fig. 2(b)). The reflections positioned at $2\theta = 38.1°$, 44.32°, 64.4°, and 77.34° correspond, to (111), (220), (311), and (400) fcc crystal planes of pure silver, respectively. For the silver shell, the calculated value of the lattice parameter from the (111) reflection is 0.408 nm. This value is in good agreement with the powder diffraction database value for bulk silver (JCPDS Card No. 04-0783) and with the values in the literature [22].

High-resolution transmission electron microscopy (HRTEM) with simultaneous EDS was employed to confirm the core–shell nature of Fe_3O_4–Ag nanostructures. Figure 3 shows the HRTEM image along with the EDS spectra of the nanostructures. The core–shell nature of the nanostructures is evidenced from the image, which is further supported by the EDS spectra. The clear light/dark contrast variation along the diameter shows that the (darker) core and (lighter) shell of the nanostructures consist of materials with different atomic masses. The EDS spectrum of the core region (marked 1) reveals that it is composed of Fe and O elements while the shell (marked 2) is populated with Ag. The detection of small amounts of Ag in the core region and Fe and O in the shell region may be due to the partial diffusion of elements in the nanostructures. It is not possible to determine the elemental ratio of Fe to Ag from the EDS spectra as they are recorded at independent locations.

Bright field TEM images along with the size distribution histograms of Fe_3O_4 nanoparticles and Fe_3O_4–Ag nanostructures are shown in Fig. 4. The Fe_3O_4 nanoparticles are nearly spherical with an average diameter of 6.2 nm + 0.7 nm. The polydispersity index of the nanoparticles is 11.3%. The Fe_3O_4–Ag nanostructures are also spherical, having an average size of 14.1 nm + 2.2 nm and polydispersity index of 15.6%. The absence of smaller size particles (<12 nm) in the TEM image of the core–shell nanostructures suggests that each Fe_3O_4 nanoparticle is coated with elemental silver, and further excludes the possibility of formation of a mixture of Fe_3O_4 and Ag nanoparticles.

The elemental concentrations of Fe and Ag were determined by inductively coupled plasma atomic emission spectroscopy (ICP-AES). The atomic concentrations of Ag and Fe found from the analysis are 702 μg/L and 216 μg/L, respectively. The mass ratio of Fe:Ag obtained in this way is used to determine the effective concentration of Ag in the core–shell nanostructure when determining the MIC values.

Figure 5 shows the UV–vis absorption spectra of Fe_3O_4–Ag nanostructures before and after phase transfer. The inset shows the absorption spectrum of Fe_3O_4 nanoparticles dispersed in hexane. In the spectrum of the core–shell nanostructures, a single surface plasmon resonance band (SPR) is observed, which originates from the elemental Ag [21, 22]. By careful analysis of the spectra, it was found that the SPR band is centered at 397.6 nm before phase transfer, while it is red-shifted to 399.6 nm after phase

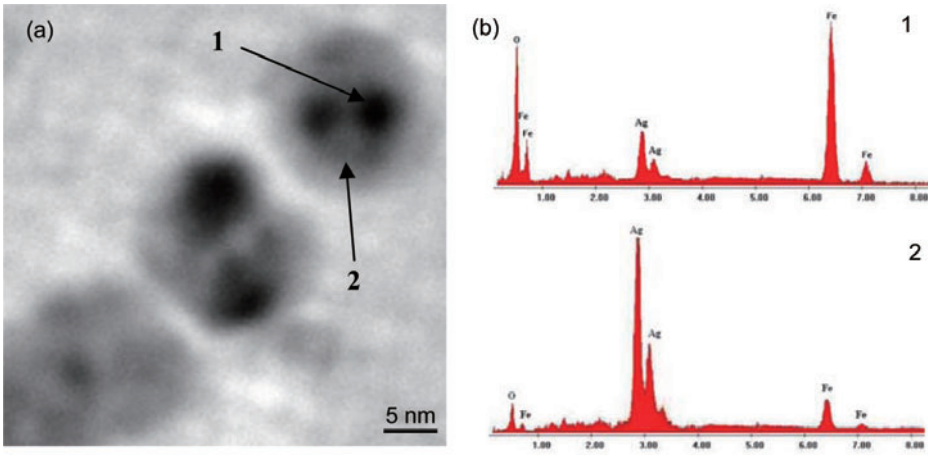

Figure 3 (a) HRTEM image of Fe_3O_4–Ag core–shell nanostructures. (b) EDS spectra from the marked regions in (a): (1) EDS spectrum of the core (dark) region and (2) EDS spectrum from the shell (light) region

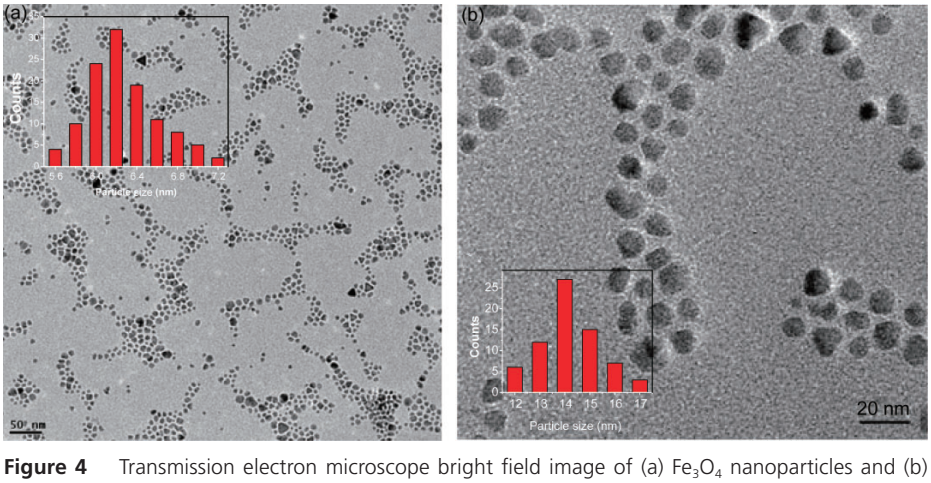

Figure 4 Transmission electron microscope bright field image of (a) Fe_3O_4 nanoparticles and (b) Fe_3O_4–Ag nanostructures. The insets show the size distribution histograms of the nanostructures

transfer. This small red shift in the phase transferred nanostructures is due to the differences in the surface adsorbed species and the dielectric medium. The position and shape of the plasmon absorption of silver nanostructures are known to be strongly dependent on the particle size, dielectric medium, and surface-adsorbed species [23, 24]. According to Mie's theory [25], only a single SPR band is expected in the absorption spectra of spherical metal nanoparticles, whereas anisotropic particles could give rise to two or more SPR bands depending on the shape of the particles. In our case, a single SPR band is observed, which suggests that our particles are spherical in shape and is consistent with the TEM observations. Furthermore, phase transfer does not alter the shape of the SPR band, which excludes the possibility of the formation of agglomerates during the phase transfer. In addition, no SPR band was observed for Fe_3O_4 alone. Hence, the presence of an SPR band in the spectrum of Fe_3O_4–Ag nanostructures is again indicative of the formation of a fine layer of a silver shell on the core of Fe_3O_4 in agreement with the results obtained from TEM and EDS analysis. The reduction in the intensity of the SPR band for the phase transferred nanostructures is due to its lower concentration.

The magnetic properties of Fe_3O_4 nanoparticles and Fe_3O_4–Ag nanostructures were also compared by magnetization measurements. Figure 6 shows the normalized magnetization curves as a function of applied external magnetic field. The observed 69% decrease in the saturation magnetization of Fe_3O_4–Ag with respect to the pure Fe_3O_4 core agrees well with the starting weight proportion (0.3:1.0) of Fe_3O_4 to Ag as well as with the results obtained from the ICP-AES analysis. Furthermore, no hysteresis and remanence were observed in the magnetization curves of Fe_3O_4 and Fe_3O_4–Ag, which indicates that the particles are superparamagnetic in nature and that the formation of a silver shell on Fe_3O_4 does not affect the superparamagnetic properties of the Fe_3O_4 core. This further leads us to conclude that the silver shell prevents agglomeration of the Fe_3O_4 nanoparticles during the formation of the core–shell nanostructures.

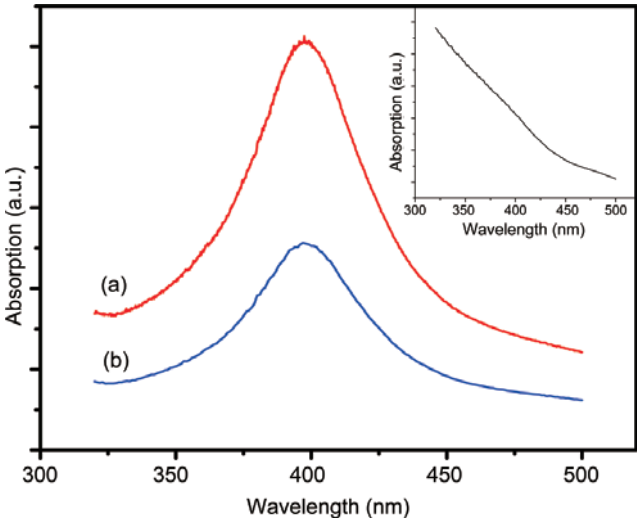

Figure 5 UV–vis spectra of Fe_3O_4–Ag core–shell nanostructures (a) before phase transfer (dispersed in hexane) and (b) after phase transfer (dispersed in water). A single SPR band centered at 397.6 nm is observed for Fe_3O_4–Ag nanostructures in hexane which is red-shifted to 399.6 nm after phase transfer. The inset shows the UV–vis spectra of Fe_3O_4 nanoparticles (dispersed in hexane)

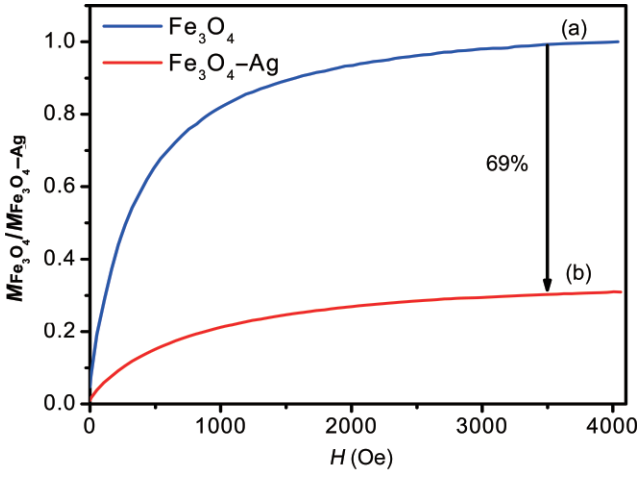

Figure 6 Normalized magnetization curves of (a) Fe_3O_4 and (b) Fe_3O_4–Ag nanostructures

2.4 Antimicrobial activity of Fe_3O_4–Ag core–shell nanostructures

Table 1 shows the MIC values of Fe_3O_4–Ag nanostructures for the tested microorganisms. The silver shell is responsible for the antimicrobial action and hence, MIC values mentioned in the table are corrected for the effective silver concentration in the core–shell nanostructure. *E. coli* was observed to be the most sensitive followed by *B. megaterium* and

Table 1 Minimum inhibitory concentration (MIC) values of Fe_3O_4–Ag core–shell nanostructures for Gram positive and Gram negative microorganisms

Microorganism	Gram positive		Gram negative	
	B. megaterium	*S. aureus*	*E. coli*	*P. vulgaris*
MIC[a] (μg/mL)	280	356	76	300

[a] MIC vales are corrected for the effective concentration of Ag in the core–shell nanostructures.

P. vulgaris. The highest MIC value was found for *S. aureus*. The table shows that there is no clear cut trend in MIC values for Gram negative and Gram positive bacteria.

Figure 7 shows a photographic view of the antibacterial tests of Fe_3O_4–Ag nanostructures against the four microorganisms. Photographs were captured after 24 h of incubation at 37 °C. For visual comparison, the test results for Fe_3O_4 nanoparticles (with a concentration equal to the MIC value of Fe_3O_4 –Ag nanostructures for the respective test organisms) are also presented (tube 4). Comparison of bacterial growth in tube 3 (without antibacterial agent) and tube 4 (with Fe_3O_4) shows that the Fe_3O_4 nanoparticles have negligible inhibitory action against the tested microorganisms. Considerable inhibition in the bacterial growth is observed when the concentration of Fe_3O_4–Ag nanostructures are 30% (tube 5) and 10% (tube 6) below the MIC value for the respective test microorganism. No bacterial growth is observed (tube 7) even after 24 h of incubation when the bacterial strains are incubated with the concentration of the Fe_3O_4–Ag nanostructures equal to the MIC. For accurate determination of the MIC, the experiments were performed at concentration intervals of 5 μg/mL.

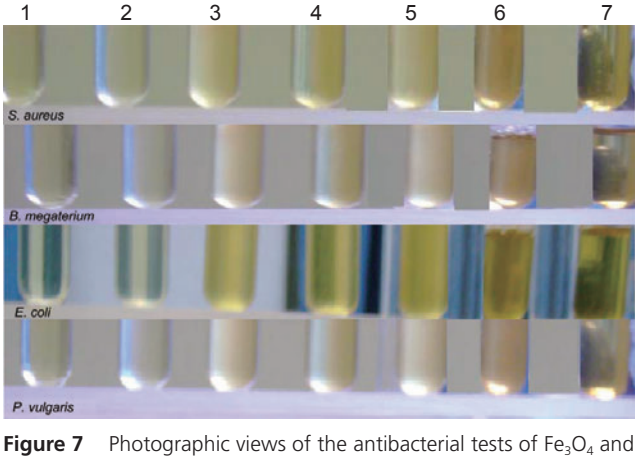

Figure 7 Photographic views of the antibacterial tests of Fe_3O_4 and Fe_3O_4–Ag nanostructures with four different microorganisms. Order of the tubes (from left to right): 1. negative control, i.e., medium alone; 2. control, i.e., medium + antibacterial agent (Fe_3O_4–Ag); 3. zero concentration, i.e., medium + respective bacterial strain; 4. controlled experiment with Fe_3O_4 (concentration was identical to the MIC value obtained with Fe_3O_4–Ag nanostructures); 5. below MIC: concentration of Fe_3O_4–Ag nanostructures was 30 % below MIC; 6. below MIC: concentration of Fe_3O_4–Ag nanostructures was 10 % below MIC; 7. at MIC

There is no known specific mechanism for the action of silver nanoparticles against different types of bacteria [26]. Interaction of silver with (i) thiol group of some vital proteins or enzymes (ii) chloride ions or (iii) nucleic acids are among the proposed modes of action for silver. Noticeable dephosphorylation of two peptides has been observed in *E. coli* and *S. typhi* exposed to silver nanoparticles [27]. As tyrosine phosphorylation in bacteria leads to activation of various protein substrates like RNA polymerase, sigma factors and uridine diphospate (UDP) glucose dehydrogenases [28], decreased phosphorylation may reflect inhibition of the activity of these enzymes with critical implications for bacterial growth. Various effects such as loss of DNA replication ability, structural changes in the cell membranes, and formation of small dense granules by Ag and S have been observed [5, 26, 29, 30].

Nanostructures introduced into the bacterial medium may act as a constant source of metal ions released by slow oxidation of the particles. Moreover, silver nanoparticles with sizes up to 10–20 nm are accumulated within living cells, thereby demonstrating an active transport across the membrane [30, 31] and function as a special biocidal agent.

MIC values reported here (for *E. coli* and *S. aureus*) are higher than those observed by Vertelov et al. [26], and lower than those recorded by Melaiye et al. [32]. Strain to strain variation in response to biocidal agents is a common occurence. Stabilization of silver

nanoparticles with Myramistin as employed by Vertelov et al. [26] could also be the reason for their high activity. The MIC value for *E. coli* in the present study is very close to those observed by Gong et al. [22].

An interesting observation is the reduction in the MIC value with Fe_3O_4–Ag core–shell nanostructures in the case of Gram negative bacteria compared to the corresponding value for silver nanoparticles. In contrast, the MIC values for Gram positive organisms for the core–shell nanostructures are the same as those observed for silver nanoparticles. These results indicate that Fe_3O_4 is playing an additive role in the inhibitory effect of silver on Gram negative organisms [33]. Gram positive bacteria lack an outer membrane but they possess a thick peptidoglycan layer (30 nm), while Gram negative organisms have an outer layer along with a thin peptidoglycan layer. Therefore, the core–shell nanostructures have to cross the outer membrane along with the thin peptidoglycan layer in Gram negative bacteria. Easy internalization of the core–shell nanostructures in the outer membrane of Gram negative bacteria could be a possible reason for the observed behavior. Decreases in MIC in the range of 100 to 400 and 200 to 400 ppm have been observed for *E. coli* and *Streptococcus epidermis*, respectively, depending on the loading of Ag nanoparticles in magnetic microspheres [33]. The MIC values recorded in the present study are much lower than the MIC values for commercially available antibacterial agents [33]. Hence, further studies of these core–shell nanostructures should be carried out in order to explore the possibility of commercial utilization.

2.5 Isolation of Fe_3O_4–Ag core–shell nanostructures from the bacterial medium

Products containing silver nanoparticles or formulations of silver are widely used as an antibacterial agent in public healthcare. Silver nanoparticles are nontoxic to humans in minute concentrations but exposure to higher doses can cause significant harm. Therefore, there are potential risks involved in using these ultra-fine silver particles for medicinal purposes, as it is very difficult to remove colloidal silver by virtue of its chemical and physical properties. Ultimately, these products end up in the environment during waste disposal and cause pollution. Therefore, it is of the utmost importance to remove these colloidal silver nanoparticles from the medium before it is released into the environment. In order to tackle this problem, we make use of the magnetic properties of the core in the core–shell nanostructures. The Fe_3O_4–Ag nanostructures were easily removed from the medium by using a steel wool filter in a static magnetic field. The medium was filtered through this metallic filter in the presence of a magnetic field, till the absorption at 399 nm in the UV–vis spectrum of the supernatant was observed. Using this simple technique it is possible to remove the colloidal silver from the bacterial medium. This method can therefore prevent the uncontrolled waste disposal of silver-based antibacterial products in the environment.

3. Conclusions

A one-pot thermal decomposition method to produce a stable aqueous suspension of narrowly dispersed highly antibacterial and superparamagnetic Fe_3O_4–Ag core–shell nanostructures has been developed. The nanostructures have demonstrated excellent antibacterial activity against both Gram negative and Gram positive organisms. Efforts have been made to understand the underlying molecular mechanism of such antimicrobial actions. The effect of the nanostructures was found to be significantly more pronounced on Gram negative strains, which suggest the additive action of the iron in the case of Gram negative microorganisms. We attribute this enhanced antibacterial activity of the nanostructures to their stability as a colloid in the medium, which results in modulation of the phosphotyrosine profile of the bacterial proteins and arrest of bacterial growth. The magnetic properties of these nanostructures were successfully utilized to isolate them from the medium and thus help in preventing contamination of the environment during waste disposal.

Acknowledgements

This work was supported by the Department of

Science and Technology (DST), New Delhi, India through the Ramanna Fellowship Scheme (No. SR/S2/RFCMP-01/2005). One of the Authors (A. K. V) is thankful to DST, New Delhi, for the FTPYS project. The authors are also grateful to the Microbiology Department of Sir. P. P. Institute of Science, Bhavnagar University, Bhavnagar, for providing the cultures. Special thanks are due to Dr. D. Srivastava, Scientist, CS&MCRI, Bhavnagar, for his help in TEM measurements.

References

[1] Kyriacou, S. V.; Brownlow, W. J.; Xu, X. -H. N. Using nanoparticle optics assay for direct observation of the function of antimicrobial agents in single live bacterial cells. *Biochemistry* **2004**, *43,* 140–147.

[2] Panacek, A.; Kvitek, L.; Prucek, R., Kolar, M.; Vecerova, R.; Pizurova, N.; Sharma, V. K.; Nevecna, T.; Zboril, R. Silver colloid nanoparticles: Synthesis, characterization, and their antibacterial activity. *J. Phys. Chem. B* **2006**, *110,* 16248–16253.

[3] Nomiya, K.; Yoshizawa, A.; Tsukagoshi, K.; Kasuga, N. C.; Hirakawa, S.; Watanabe, J. Synthesis and structural characterization of silver(Ⅰ), aluminium(Ⅲ) and cobalt(Ⅱ) complexes with 4-isopropyltropolone (hinokitiol) showing noteworthy biological activities. Action of silver(Ⅰ)-oxygen bonding complexes on the antimicrobial activities. *J. Inorg. Biochem.* **2004**, *98,* 46–60.

[4] Gupta, A.; Silver, S. Molecular genetics: Silver as a biocide: Will resistance become a problem? *Nat. Biotechnol.* **1998**, *16,* 888–1098.

[5] Feng, Q. L.; Wu, J.; Chen, G. Q.; Cui, F. Z.; Kim, T. N.; Kim, J. O. A mechanistic study of the antibacterial effect of silver ions on *Escherichia coli* and *Staphylococcus aureus*. *J. Biomed. Mater. Res.* **2002**, *52,* 662–668.

[6] Holladay, R.; Moeller, W.; Mehta, D.; Brooks, J.; Roy, R.; Mortenson, M. Silver/water, silver gels and silver-based compositions; And methods for making and using the same. Patent, Pub. No. WO/2006/074117, July 13, 2006; International Application No. PCT/US2005/047699, Dec. 30, 2005.

[7] Rosenman, K. D.; Moss, A.; Kon, S. Argyria: Clinical implication of exposure to silver nitrate and silver oxide. *J. Occup. Med.* **1979**, *21,* 430–435.

[8] Cohen, S. Y.; Quentel, G.; Egasse, D.; Cadot, M.; Ingster-Moati, I.; Coscas, G. J. The dark choroid in systemic argyrosis. *Retina* **1993**, *13,* 312–316.

[9] Rungby, J. An experimental study on silver in the nervous system and on aspects of its general cellular toxicity. *Dan. Med. Bull.* **1990**, *37,* 442–449.

[10] Chopra, I. The increasing use of silver-based products as antimicrobial agents: A useful development or a cause for concern? *J. Antimicrob. Chemoth.* **2007**, *59,* 587–590.

[11] Asharani, P. V.; Wu, Y. L.; Gong, Z. Y.; Valiyaveettil, S. Toxicity of silver nanoparticles in zebrafish models. *Nanotechnology,* **2008**, *19,* 255102.

[12] WHO. *Guidelines for Drinking-Water Quality;* World Health Organization: Geneva, 1998. Vol. 2, p. 338.

[13] Drake, P. L.; Hazelwood, K. J. Exposure-related health effects of silver and silver compounds: A review. *Ann. Occup. Hyg.* **2005**, *49,* 575–585.

[14] Sun, S. H.; Zeng, H. Size-controlled synthesis of magnetite nanoparticles. *J. Am. Chem. Soc.* **2002**, *124,* 8204–8205.

[15] Sun, S. H.; Zeng, H.; Robinson, D. B.; Raoux, S.; Rice, P. M.; Wang, S. X.; Li, G. X. Monodisperse MFe_2O_4 (M = Fe, Co, Mn) nanoparticles. *J. Am. Chem. Soc.* **2004**, *126,* 273–279.

[16] Toshima, N.; Yonezawa, T.; Kushihashi, K. Polymer-protected palladium–platinum bimetallic clusters: Preparation, catalytic properties and structural considerations. *J. Chem. Soc. Faraday Trans.* **1993**, *89,* 2537–2543.

[17] Liz-Marzan, L. M.; Philipse, A. P. Stable hydrosols of metallic and bimetallic nanoparticles immobilized on imogolite fibers. *J. Phys. Chem.* **1995**, *99,* 15120–15128.

[18] Esumi, K.; Tano, T.; Torigoe, K.; Meguru, K. Preparation and characterization of bimetallic palladium-copper colloids by thermal decomposition of their acetate compounds in organic solvents. *Chem. Mater.* **1990**, *2,* 564–567.

[19] Mafune, F.; Kohnok, J.; Takeda, Y.; Kondow, T.; Sawabe, H. Structure and stability of silver nanoparticles in aqueous solution produced by laser ablation. *J. Phys. Chem. B* **2000**, *104,* 8333–8337.

[20] Hiramatsu, H.; Osterloh, F. E. A simple large-scale synthesis of nearly monodisperse gold and silver nanoparticles with adjustable sizes and with exchangeable surfactants. *Chem. Mater.* **2004**, *16,* 2509–2511.

[21] Chen, M.; Feng, Y. G.; Wang, X.; Li, T. C.; Zhang, J. Y.;

Qian, D. J. Silver nanoparticles capped by oleylamine: Formation, growth, and self-organization. *Langmuir* **2007**, *23,* 5296–5304.

[22] Gong, P.; Li, H. M.; He, X. X.; Wang, K. M.; Hu, J. B.; Tan, W. H.; Zhang, S. C.; Yang, X. H. Preparation and antibacterial activity of Fe_3O_4@Ag nanoparticles. *Nanotechnology* **2007**, *18,* 285604.

[23] Kewibig, U.; Vollmer, M. *Optical Properties of Metal Clusters;* Springer: Berlin, 1995.

[24] Mulvaney, P. Surface plasmon spectroscopy of nanosized metal particles. *Langmuir* **1996**, *12,* 788–800.

[25] Novak, J. P.; Feldheim, D. L. Assembly of phenylacetylene-bridged silver and gold nanoparticle arrays. *J. Am. Chem. Soc.* **2000**, *122,* 3979–3980.

[26] Vertelov, G. K.; Krutyakov, Y. A.; Efremenkova, O. V.; Olenin, A. Y.; Lisichkin, G. V. A versatile synthesis of highly bactericidal Myramistin® stabilized silver nanoparticles. *Nanotechnology* **2008**, *19,* 355707.

[27] Shrivastava, S.; Bera, T.; Roy, A.; Singh, G.; Ramachandrarao, P.; Dash, D. Characterization of enhanced antibacterial effects of novel silver nanoparticles. *Nanotechnology* **2007**, *18,* 225103.

[28] Mijakovic, I.; Petranovic, D.; Bottini, N.; Deutscher, J.; Jensen, P. R. Protein-tyrosine phosphorylation in *Bacillus subtilis*. *J. Mol. Microb. Biotech.* **2005**, *9,* 189–197.

[29] Nover, L.; Scharf, K.D.; Neumann, D. Formation of cytoplasmic heat shock granules in tomato cell cultures and leaves. *Mol. Cell Biol.* **1983**, *3,* 1648–1655.

[30] Morones, J. R.; Elechegueerra, J. L.; Camacho, A.; Holt, K.; Kouri, J. B.; Ramirez, J. T.; Yacaman, M. J. The bactericidal effect of silver nanoparticles. *Nanotechnology* **2005**, *16,* 2346–2353.

[31] Raffi, M.; Hussain, F.; Bhatti, T. M.; Akhter, J. I.; Hameed, A.; Hasan, M. M. Antibacterial characterization of silver nanoparticles against *E. coli* ATCC-15224. *J. Mater. Sci. Technol.* **2008**, *24,* 192–196.

[32] Melaiye, A.; Sun, Z. H.; Hindi, K.; Milsted, A.; Ely, D.; Reneker, D. H.; Tessier, C. A.; Youngs, W. J. Silver(I)–imidazole cyclophane gem-diol complexes encapsulated by electrospun tecophilic nanofibers: Formation of nanosilver particles and antimicrobial activity. *J. Am. Chem. Soc.* **2005**, *127,* 2285–2291.

[33] Lee, D.; Cohen, R. E.; Rubner, M. F. Antibacterial properties of Ag nanoparticle loaded multilayers and formation of magnetically directed antibacterial microparticles. *Langmuir* **2005**, *21,* 9651–9659.